Taylor & Francis
Taylor & Francis Group

Experimental Heat Transfer

A Journal of Thermal Energy Generation, Transport, Storage, and Conversion

ISSN: (Print) (Online) Journal homepage: https://www.tandfonline.com/loi/ueht20

Experimental hydrothermal characteristics of concentric tube heat exchanger with V-cut twisted tape turbulator using PCM dispersed mono/hybrid nanofluids

Sumit Kr. Singh & Jahar Sarkar

To cite this article: Sumit Kr. Singh & Jahar Sarkar (2020): Experimental hydrothermal characteristics of concentric tube heat exchanger with V-cut twisted tape turbulator using PCM dispersed mono/hybrid nanofluids, Experimental Heat Transfer

To link to this article: https://doi.org/10.1080/08916152.2020.1772412

Published online: 16 Jun 2020.

Submit your article to this journal

View related articles

View Crossmark data

Full Terms & Conditions of access and use can be found at
https://www.tandfonline.com/action/journalInformation?journalCode=ueht20

EXPERIMENTAL HEAT TRANSFER
https://doi.org/10.1080/08916152.2020.1772412

Taylor & Francis
Taylor & Francis Group

Check for updates

Experimental hydrothermal characteristics of concentric tube heat exchanger with V-cut twisted tape turbulator using PCM dispersed mono/hybrid nanofluids

Sumit Kr. Singh and Jahar Sarkar

Department of Mechanical Engineering, Indian Institute of Technology (B.H.U.), Varanasi, India

ABSTRACT

Impact of using V-cuts twisted tape insert and phase change material (PCM) dispersed mono or hybrid nanofluid on the hydrothermal characteristics of the double tube heat exchanger is experimentally investigated. Water-based Al_2O_3 and PCM nanofluids and Al_2O_3+ PCM hybrid nanofluid with different concentrations are used in inner tube. Influences of various geometric parameters of V-cuts twisted tape insert on heat transfer, pressure drop and entropy generation are investigated. Results reveal that heat transfer and pressure drop increase with the increase in particle concentration and decrease in twisting ratio. A higher V-cut depth ratio or lower width ratio yields more heat transfer and pressure drop.

ARTICLE HISTORY
Received 6 April 2020
Accepted 18 May 2020

KEYWORDS
hybrid nanofluid; phase change material; V-cuts twisted tape; heat transfer coefficient; pressure drop; entropy generation

Introduction

The double tube heat exchanger is broadly used in various industrial and commercial applications and hence it requires the improvement in heat transfer and fluid flow characteristics. The enhancement methods developed for heat exchanger are mainly classified as active and passive methods. Among them, passive techniques are more beneficial than active techniques as there is no requirement of external power and are easy to implement at a lower cost. Hence, many passive methods have been used and integrated into double tube heat exchanger including wire coil inserts [1–3], louvered strip inserts [4,5], conical strip inserts [6], conical ring inserts [7,8], delta wing vortex generators [9–11], lanced ring insert [12], wavy strip [13], conventional-twisted tape inserts [14–18], V-cut twisted tape inserts with different modification [19–24] and compound inserts [25]. Among the passive methods, the twisted tape insertion is widely used in the heat exchanger as it is easy to assemble and disassemble, easy to manufacture and has a relatively lower pressure drop among all inserts. It also provides a large surface area, forms a swirl flow inside the pipe and creates turbulence near to the wall. Another passive option to improve thermal performance is to use nanofluid instead of conventional fluid. Many authors employed the nanofluids in various engineering applications such as solar energy [26–29], automotive industry [30], heat exchanger [31], electronic cooling [32,33], natural circulation loop [34] and refrigeration systems [35]. The improvement in heat transfer using nanofluids mainly causes by the effects of different mechanisms such as nanoparticle Brownian motion, particle interface liquid layering, heat transport between nanoparticles and nanoparticle clustering as well as superior thermal conductivity. Recently, the phase change material (PCM) suspension as heat transfer fluids has gained a special interest in heat transfer application [36]. Suspension of nanoparticles enhances thermal conductivity but reduces heat capacity; whereas, suspension of PCM may reduce thermal conductivity but enhances overall heat capacity because of its latent heat during phase change [37]. Hence, the suspension of both nanoparticle and PCM in the base fluid can trade-off between individual

CONTACT Jahar Sarkar jsarkar.mec@itbhu.ac.in
© 2020 Taylor & Francis

advantages and disadvantages, and this hybrid nanofluid can exhibit overall thermal performance improvement of the heat exchanger, which is the main motivation behind the present study.

Several research works were reported in the literature on heat exchanger using nanofluid and twisted tape inserts. Maddah et al. [38] experimented on the heat transfer behavior of Al_2O_3/water nanofluids in a double tube heat exchanger equipped with modified twisted tape and reported 12% to 52% performance enhancement depending on geometrical progression ratio. Esmaeilzadeh et al. [39] investigated thermal performance by inserting twisted tape inserts with varying thicknesses in the tube using Al_2O_3/water nanofluid and found that thicker tape offers better heat transfer characteristics. Prasad et al. [40] investigated the heat exchange behavior of Al_2O_3/water nanofluid in double tube U-bend heat exchanger by inserting trapezoidal-cut twisted tape and reported 34.2% average Nusselt number improvement. Hazbehian et al. [41] experimented on the thermal behavior of concentric tube heat exchanger with twisted tape inserts by flowing polymeric nanofluid and found that both heat exchange and pressure drop increase with the increase in twist width. Nakhchi and Esfahani [42] numerically studied the Cu/water nanofluid flowing in the circular tube by inserting a cross-cut twisted tape turbulator and showed higher thermal performance as compared to that with conventional twisted tape insert. Khoshvaght-Aliabadi et al. [43] used spiky-twisted tape inserted in a U-shaped heat exchanger to investigate the hydrothermal characteristics using different nanofluids and found that with spiky-twisted tapes, Ag/water nanofluid shows the maximum improvement in heat transfer coefficient by 18.2% with respect to only water. Bahiraei et al. [44] did a numerical study on the combined effects of double-twisted tape and hybrid nanofluid flowing in tubes and showed that the twisted tapes of the counter arrangement provide lower entropy generation rate as compared to that of parallel arrangement. Eiamsa-ard et al. [45] studied experimentally the thermo-hydraulic behaviors of a dimpled tube mounted with twisted tape inserts using TiO_2/water nanofluid and found a strong influence of dimple angle, twist ratio, and nanofluid concentration. Recently, Singh and Sarkar [46] experimentally studied the hydrothermal characteristics on a double tube heat exchanger inserted with V-cuts twisted tape using Al_2O_3+ TiO_2 hybrid nanofluid and reported significant thermal performance improvement. However, with the best of the authors' knowledge, there is no reported investigation with modified twisted tape insert for PCM dispersed mono or hybrid nanofluids.

Hence, the present study reports the experimental study on double tube heat exchanger with V-cuts twisted tape inserts and PCM dispersed mono and hybrid nanofluids flowing in the inner tube. Effects of Al_2O_3-PCM mixture ratio, total volume concentration on heat transfer and pressure drop characteristics have been investigated. The effects of twisted tape geometric parameters such as twist ratio, depth ratio, and width ratio on the hydrothermal performances have also been analyzed. Additionally, the ratio heat transfer coefficient to pressure drop and entropy generation have been reported as well to illustrate the effects of V-cuts twisted tape inserts and hybrid nanofluids on these parameters.

Experimental investigation

Nanofluid preparation and characterization

Water-based mono and hybrid nanofluids were prepared by using the two-step method. Al_2O_3 nanoparticle of average size <50 nm was purchased from Otto Chemika. Figure 1 shows the SEM image of Al_2O_3 nanofluid and exposes that the nanoparticles are of spherical shape and the average size of 50 nm. In this study, capric acid was used as PCM because of its physical properties. The melting point of capric acid is slightly above room temperature (~32°C) and having high latent heat. Al_2O_3 nanoparticle and phase change material were used and their properties are given in Table 1. The nanoparticle volume concentrations of 0.01% and 0.1% were used for synthesizing the nanofluids. For hybrid nanofluid, the particles (Al_2O_3+ PCM) were taken in a 50/50 ratio. The nanoparticles were first dispersed in 10 L water and then the solution was sonicated for 180 min using ultrasonicator (Labman Scientific Instruments) of power 200 W at 40 kHz. The temperature was maintained above 40°C to get

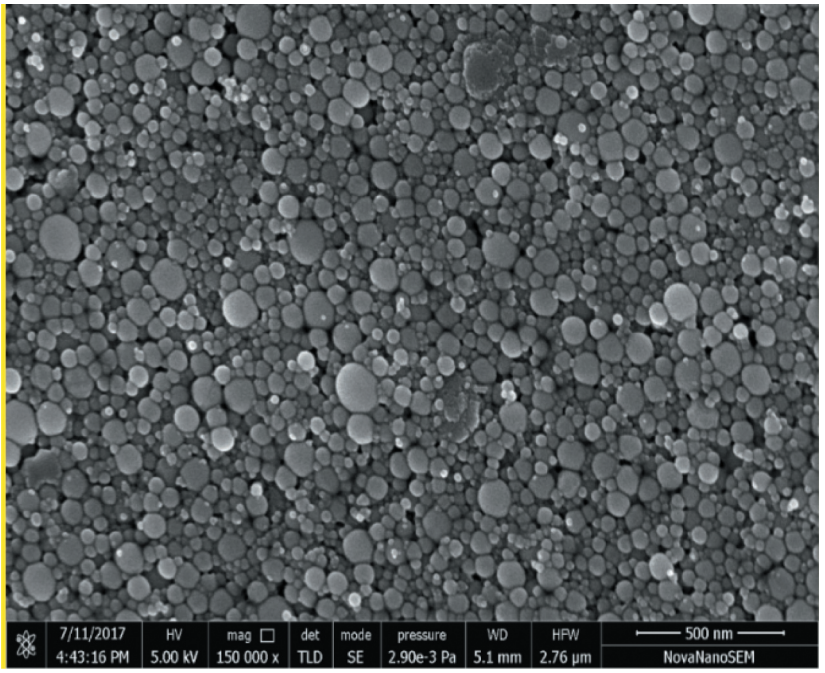

Figure 1. SEM image of Al_2O_3 nanoparticles.

Table 1. Thermo-physical properties of the base fluid, nanoparticle and PCM.

Materials	Thermal conductivity (W/mK)	Density (kg/m^3)	Specific heat (J/kg.K)	Viscosity (Pa.s)	Melting point (^oC)	Latent heat (kJ/kg)
Water	0.606	995	4183	0.0007623	-	-
Al_2O_3	40	3900	880	-	-	-
PCM	0.151 (liquid)	1004 (solid) 870 (liquid)	2100 (solid) 2090 (liquid)	-	31.6	157.8

dispersion of PCM in liquid form. Both specific heat capacity and thermal conductivity of prepared nanofluids were measured by thermal constants analyzer (Model: TPS-500, Hot Disk Instruments). The dynamic viscosity of prepared nanofluids was measured by a digital viscometer (Model: LVDV-II+ Pro, Brookfield Inc.). The density of prepared nanofluids was estimated by measuring the mass of certain volume using a high precision digital weighing balance (model: ATX224, Shimadzu, Japan) followed by the relation, density = mass/volume. The visual observation of the mono/hybrid nanofluids was done to ensure the stability of nanofluid, as shown in Figure 2. The sedimentation occurred after 10 days, which was enough time interval for conducting required experiments. Additionally, the pH value of synthesized mono/hybrid nanofluids was measured using a digital pH meter. Its value was found far away from the nanoparticle's isoelectric point. Moreover, all properties of mono/hybrid nanofluids were estimated before and after the experiment to inspect their stability. All measured properties were found with insignificant differences. These tests also confirmed the stability of studied mono/hybrid nanofluids.

Setup description and method

The schematic and actual diagrams of the experimental apparatus, where the experiments were conducted, are shown in Figure 3(a) and (b), respectively. It mainly consists of the concentric tube

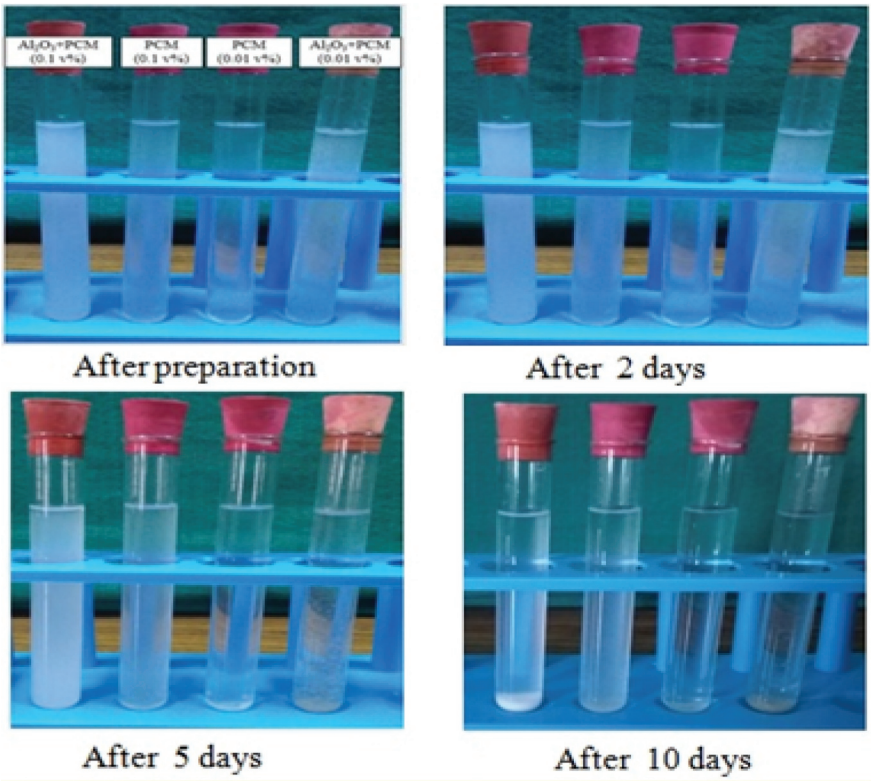

Figure 2. Visual observation of mono and hybrid nanofluids.

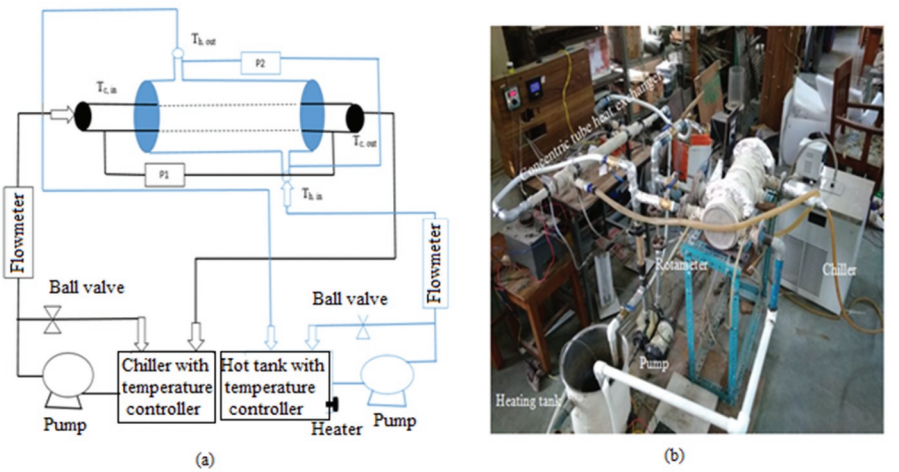

Figure 3. (a) Schematic diagram of the experimental setup (b) Actual picture of test setup.

heat exchanger, heating tank with temperature controller, cooling tank (chiller) with temperature controller, two rotameters, two centrifugal pumps and U-tube manometers. This experimental setup contains two working fluid forced circulation loops of hot fluid (DI water) and cold fluid (mono/hybrid nanofluid). The mono/hybrid nanofluid flow was through the inner tube and the hot DI water

flow was through the outer tube (annulus) in the opposite direction. Two centrifugal pumps of 80 W each were used to drive both fluids in the heat exchanger. The required hot fluid inlet temperature was adjusted by an electric heater attached to the heating tank with a temperature controller. The cold tank/chiller of 3 kW cooling capacity with a temperature controller was used for cooling the warm hybrid nanofluid and maintaining the required inlet temperature. The internal and external diameters of the inner tube are 18 and 26 mm, respectively, while the outer tube has an internal diameter 47 mm. Asbestos rope as an insulating material was wrapped over the outer tube to minimize the heat losses to the environment. Four calibrated PT100 thermocouples were provided at the inlet and exit ports of the hot and cold fluids for measuring the temperatures. The volumetric flow rates of both hot and cold fluids were controlled by adjusting the ball valve. All the readings were recorded after reaching the steady-state.

Various V-cut twisted tapes used in the present study are shown in Figure 4. Twist ratios (TR, defined as H/D; where H is the pitch and D is the width of the tape) of 5, 10, and 15 have been used. The twisted tapes are made of the aluminum strip with thickness and width of 1 mm and 15 mm, respectively. V-cuts with different depth and width were made at both sides of the plain twisted tapes. Two different depth ratios (DR = Pe/D) of 1/2 and 1/3, and two different width ratios (WR = w/D) of 1/2 and 1/3 have been used. Hence, the following V-cut configuration combinations were used in this study: (i) DR = 1/2 and WR = 1/2, (ii) DR = 1/3 and WR = 1/2, and (iii) DR = 1/2 and WR = 1/3.

The geometric data of the studied concentric tube heat exchanger, as well as used various V-cuts twisted tapes and operating conditions are provided in Table 2. The hot fluid was supplied through annulus at a constant temperature of 60°C with a constant flow rate of 15 lpm (to maintain the turbulent condition). The inlet temperature of the mono or hybrid nanofluid was maintained at 30°C (normal ambient temperature in India). The cold stream flow rate was maintained, ranging from 5 to 25 lpm (with Reynolds number ranging from 8000 to 40000). The reasons for taking this operating range are achieving a turbulent flow regime and less studied range. Before the data analysis, all the

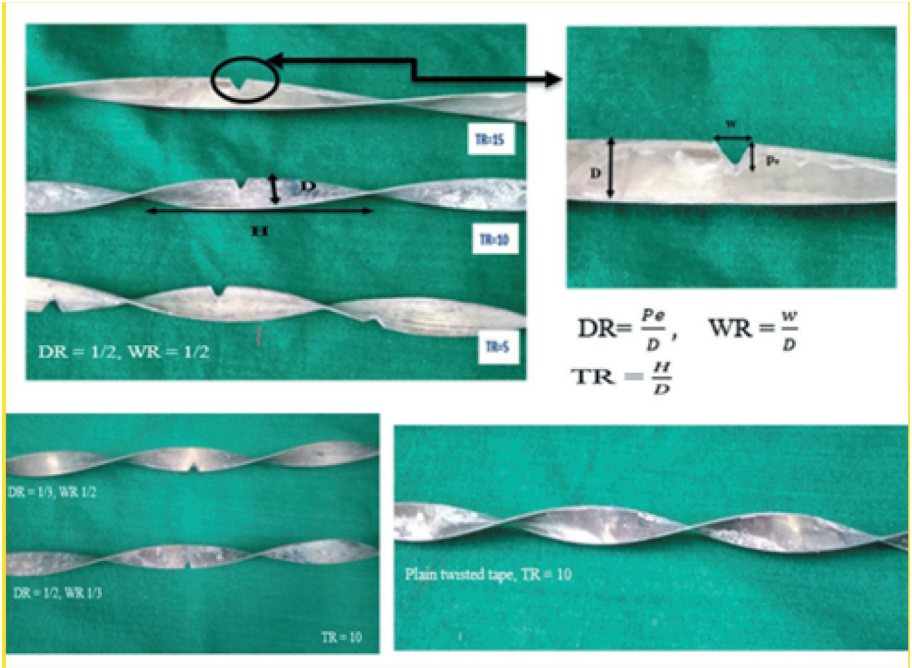

Figure 4. V-cuts twisted tape with different TR, DR, and WR.

Table 2. Details of the experimental setup and operating conditions.

Parameter	Value
Inner tube internal diameter	18 mm
Inner tube external diameter	26 mm
Length of the tube	570 mm
Outer tube internal diameter	47 mm
Tape width	15 mm
Tape thickness	1 mm
Twist ratio (TR = H/D)	5, 10 and 15
Depth of the V-cuts (P_e)	5 and 7.5 mm
Width of the V-cuts (w)	5 and 7.5 mm
Depth ratio (DR = P_e/D)	1/2 and 1/3
Width ratio (WR = w/D)	1/2 and 1/3
Nanofluid flow rate	5–25 lpm
Reynolds number (Re)	8000–40000
Nanofluid inlet temperature	30°C
Hot fluid inlet temperature	60°C

experiments were repeated two times for each data set (no substantial differences in readings were observed) and the average of these two values was taken for the calculation.

Data reduction

Hybrid nanofluid heat transfer rate in the inner tube is calculated by,

$$Q_{hnf} = \dot{V}\,\rho_{hnf} c_{p_{hnf}} \left(T_{c,out} - T_{c,in}\right) \tag{1}$$

In the case of phase change material (PCM), the mono/hybrid nanofluid heat transfer rate (melting temperature in between inlet and exit temperatures) is calculated by,

$$Q_{hnf} = \dot{V}\,\rho_{hnf} c_{p_{hnf}} \left(T_{c,out} - T_{c,in}\right) + \varphi_{PCM}\,\dot{V}\,\rho_{PCM,solid} L_{PCM} \tag{2}$$

Where L is the latent heat of the PCM.

Hot fluid (DI water) heat transfer rate in outer tube is calculated by,

$$Q_h = \dot{V}_h\,\rho_h c_{ph} \left(T_{h,in} - T_{h,out}\right) \tag{3}$$

The average heat transfer rate is determined by,

$$Q_{avg} = \left(Q_{hnf} + Q_h\right)/2 \tag{4}$$

Equation (5) is used to estimate the overall heat transfer coefficient for inner tube side,

$$U_i = \frac{Q_{avg}}{A_i \times LMTD},\ LMTD = \frac{\left(T_{h,in} - T_{c,out}\right) - \left(T_{h,out} - T_{c,in}\right)}{\ln\left(\frac{T_{h,in} - T_{c,out}}{T_{h,out} - T_{c,in}}\right)} \tag{5}$$

Heat transfer coefficient (hybrid nanofluid) without considering fouling can be estimated by,

$$\frac{1}{U_i A_i} = \frac{1}{h_i A_i} + \frac{\ln(d_o/d_i)}{2\pi KL} + \frac{1}{h_o A_o} \tag{6}$$

Nusselt number of annulus side is calculated by Dirker and Mayer correlation [47],

$$Nu_o = 0.007435 \mathrm{Re}^{0.91} \mathrm{Pr}^{1/3} \left(\frac{\mu}{\mu_w}\right)^{0.14} \tag{7}$$

Range: 4000 < Re <30000, 1.72 < $d_{ot,\ i}/d_{it,o}$ < 3.2

Then, the heat transfer coefficient in outer tube has been evaluated by,

$$h_o = Nu_o \frac{k_o}{d_{eqv}} \tag{8}$$

Where $d_{eqv}$is the equivalent diameter of annulus and calculated by,

$$d_{eqv} = \left(d_{ot,i}{}^2 - d_{it,o}{}^2\right)/d_{it,o} \tag{9}$$

Then, the heat transfer coefficient of inner tube flow has been estimated by using Eq. (6). The Nusselt number of hybrid nanofluid can be evaluated by the following equation:

$$Nu_{hnf} = h_{hnf} d_{it,i}/k_{hnf} \tag{10}$$

Expression for the evaluation of friction factor is as follows;

$$f = \frac{\pi^2}{8} \Delta \mathrm{p} \left(\frac{\rho_{\mathrm{hnf}} \mathrm{d_{it,i}}^2}{\dot{\mathrm{m}}_{\mathrm{hmf}}{}^2 \mathrm{L}} \right) \tag{11}$$

Total entropy generation for the heat exchange device has been evaluated by;

$$S_{gen} = m_c c_{p_c} \ln\left(\frac{T_{c,out}}{T_{c,in}}\right) + \frac{m_c \Delta \mathrm{p_c}}{\rho_c T_{avg,c}} + m_h c_{p_h} \ln\left(\frac{T_{h,out}}{T_{h,in}}\right) + \frac{m_h \Delta \mathrm{p_h}}{\rho_h T_{avg,h}} \tag{12}$$

Uncertainty analysis

Using error of measured parameters (x), the uncertainty of obtained parameters (X) can be estimated by using equations developed by Kline and McClintock [48].

$$\frac{\delta X}{X} = \sqrt{\left(\frac{\delta x_1}{x_1}\right)^2 + \left(\frac{\delta x_2}{x_2}\right)^2 + - - - - - - + \left(\frac{\delta x_n}{x_n}\right)^2} \tag{13}$$

Appendix A presents the complete details for the evaluation of the uncertainty values of the obtained parameters. Uncertainties of measured parameters and based on the accuracies of measured variables and properties, the uncertainty values of estimated parameters such as Re, Q, U, h, Nu, f, S_{gen} are presented in Table 3.

Table 3. Uncertainty of parameters.

Parameter	Uncertainty (%)
Temperature, T	±0.33
Density, ρ	±1
Viscosity, μ	±1
Thermal conductivity, k	±1
Reynolds number, Re	±1.22
Heat transfer rate, Q	±1.27
Overall heat transfer coefficient, U	±1.31
Heat transfer coefficient, h	±2.13
Nusselt number, Nu	±2.35
Friction factor, f	±6.45
Entropy generation, S_{gen}	±6.10

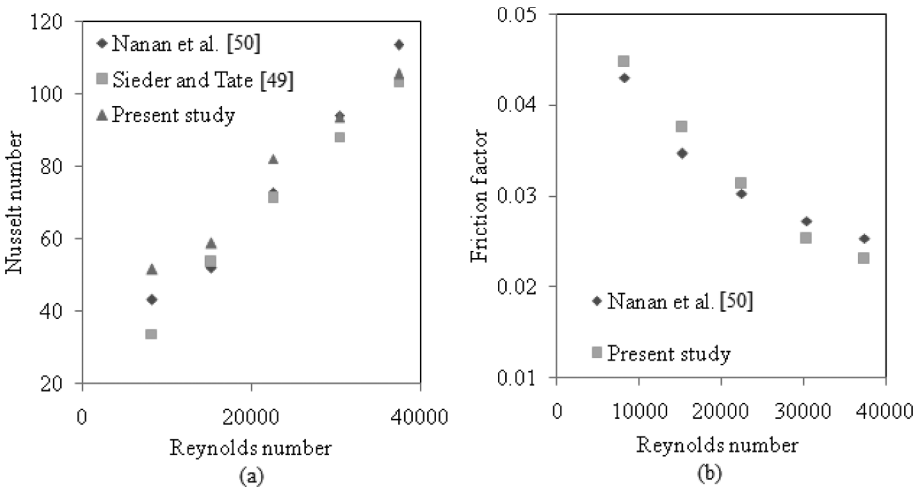

Figure 5. Validation of (a) Nussult number and (b) friction factor using water with plain tube.

Validation for water

In the beginning, the experiment was conducted with plain tube (without inserts) using DI water and the results obtained were validated with standard correlations of Sieder-Tate [49] and Nanan et al. [50] for Nusselt number and that of Nanan et al. [50] for friction factor as shown in Figure 5(a) and (b).

Sieder and Tate [49] correlation;

$$Nu = 0.027Re^{0.8}Pr^{0.33}\left(\frac{\mu}{\mu_s}\right)^{0.14} \tag{14}$$

Nanan et al. [50] correlations;

$$Nu = 0.0068Re^{0.92}Pr^{0.4} \tag{15}$$

$$f = 1.01Re^{-0.37} \tag{16}$$

The experimental Nu and f were calculated using equation (10) and (11). The results show that the experimental data are in reasonable agreement with the Sieder-Tate and Nanan et al. correlations for Nusselt number with an average deviation of $\pm$ 12.9% and $\pm$ 9.5%, respectively. The friction factor is also agreed well with the Nanan et al. correlation with an average deviation of $\pm$ 6.4%. Moreover, to gain confidence in the experimental data, the experimental apparatus was also validated by performing the experiments with DI water flowing in the tube inserted with the plain twisted tape of TR = 10. The experimental outcomes were compared with the correlations (17) and (18) proposed by Manglik and Bergles [51] as predicted in Figures 6 and 7. It can be concluded that the experimental data were in good agreement with the correlations and exhibited a maximum deviation of 5.68% for Nusselt number and 5.55% for friction factor.

$$Nu = \left(1 + \frac{0.769}{TR}\right)\left[0.023\mathrm{Re}^{0.8}\mathrm{Pr}^{0.4} \times \left(\left(\frac{\pi}{\pi - \left(\frac{4\delta}{d_i}\right)}\right)^{0.8}\left(\frac{\pi + 2 - \left(\frac{2\delta}{d_i}\right)}{\pi - \left(\frac{4\delta}{d_i}\right)}\right)^{0.2}\right)\right] \tag{17}$$

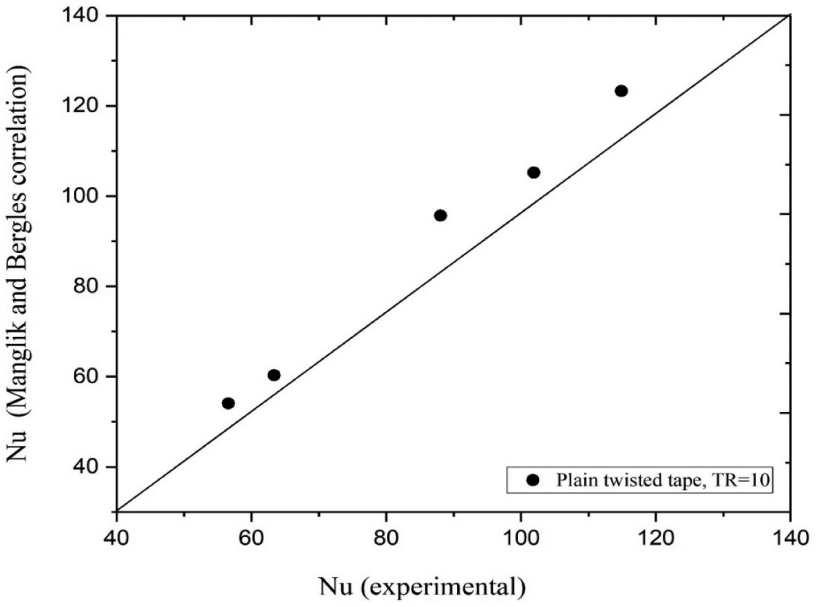

Figure 6. Validation of Nussult number using water with plain twisted tape.

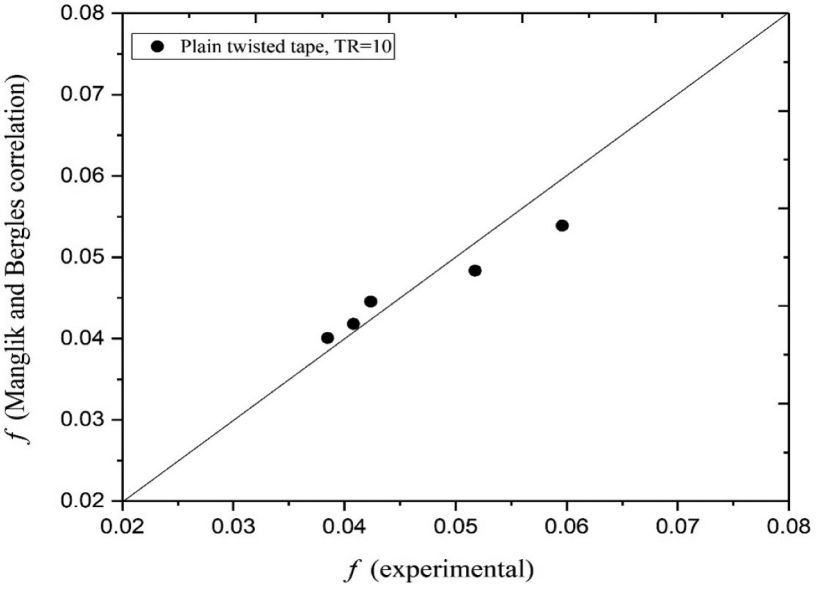

Figure 7. Validation of friction factor using water with plain twisted tape.

$$f = \left(1 + 2.06\left(1 + \left(\frac{2TR}{\pi}\right)^2\right)^{-0.74}\right)\left[0.079\mathrm{Re}^{-0.25} \times \left(\frac{\pi}{\pi - \left(\frac{4\delta}{d_i}\right)}\right)^{1.75}\left(\frac{\pi + 2 - \left(\frac{2\delta}{d_i}\right)}{\pi - \left(\frac{4\delta}{d_i}\right)}\right)^{1.25}\right] \quad (18)$$

Where δ is the tape thickness.

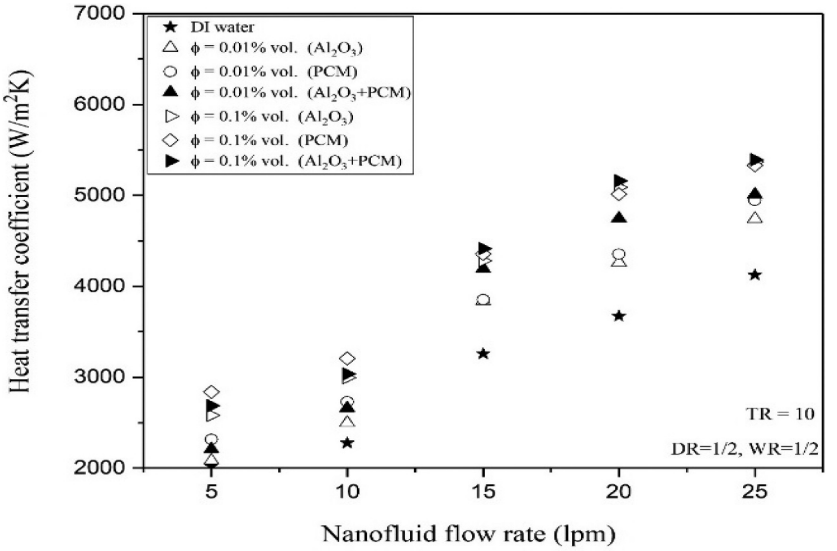

Figure 8. Variation of heat transfer coefficient with nanofluid flow rate for different volume concentrations.

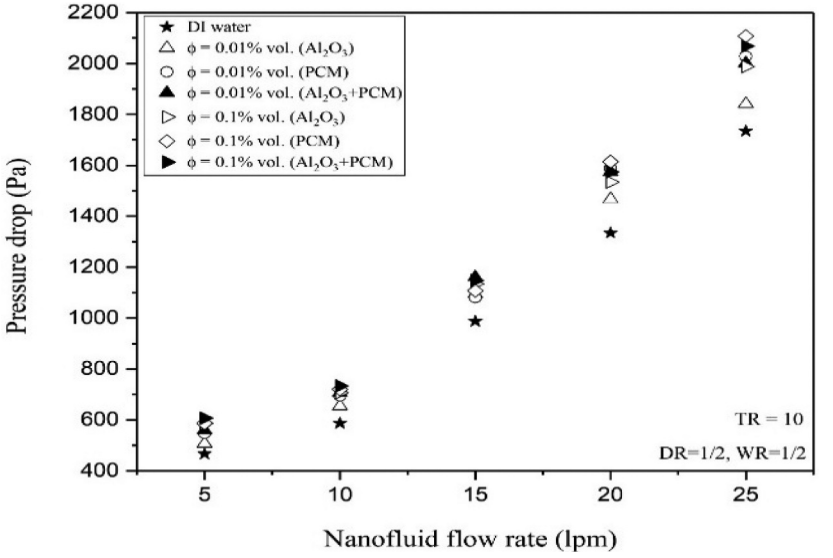

Figure 9. Variation of pressure drop with nanofluid flow rate for different volume concentrations.

Findings and discussion

Effect of particle volume concentration

Figures 8 and 9 show the influence of volume concentration of nanofluid on heat transfer coefficient (h_i) and pressure drop (Δp) with mean twist ratio (TR = 10) and constant depth and width ratios (DR = 1/2, WR = 1/2). The results indicate that h_i and Δp increase considerably with the increase in the nanofluid flow rate (Reynolds number from 10000 to 35000). In addition, both h_i and Δp are higher as compared to those of the DI water and enhance with the increase in volume concentration. Both the thermal conductivity and fluid viscosity

increase by adding the nanoparticles in the base fluid, which are the key factors for the enhancement of the pressure drop and heat transfer. Due to nanoparticle collision and the pseudoplastic behavior of the nanofluid, the thermal conductivity enhances. The apparent viscosity of the nanofluid decreases due to the higher shear rate near the wall, which leads to diminishes the boundary layer and thus augments the heat transfer. The shear force, acting on the wall, increases due to the presence of nanoparticles, which causes an increase of pressure drop. The maximum value of h_i and Δp is observed 5392.5 W/m^2 K for Al_2O_3+ PCM hybrid nanofluid and 2107.9 Pa for PCM, respectively, at a higher flow rate (25 lpm) and 0.1% volume concentration. Also, the increments of about 25.62% in heat transfer coefficient for Al_2O_3+ PCM hybrid nanofluid and 16.05% in pressure drop for PCM are observed as compared to DI water. When the volume concentration increases from 0.01% to 0.1%, the maximum augmentations of 10.05% in the heat transfer coefficient for Al_2O_3+ PCM and 5.96% in pressure drop for PCM are found at a flow rate of 25 lpm. Also, the results show that PCM yields a higher heat transfer coefficient at a low flow rate. The coolant has a longer time to absorb heat from the hot fluids at a low flow rate and increases the phase change processes completely, which increases the heat transfer of the coolant and heat storage in PCM particles as the latent heat. At a higher flow rate, PCM shows higher pressure drop due to increased viscosity with the addition of phase change particles.

Figures 10 and 11 predict the variations of $h_i/\Delta p$ ratio and entropy generation with respect to the nanofluid flow rate. As shown in Figure 10, the $h_i/\Delta p$ ratio decreases with an increase in the nanofluid flow rate for all cases of working fluids. The $h_i/\Delta p$ ratio yields maximum value at a low flow rate as h_i dominances over Δp at a low flow rate. Also, all working fluids of 0.1% volume concentration have a higher $h_i/\Delta p$ ratio than working fluids of 0.01% volume concentration. Among all working fluids, PCM nanofluid shows maximum $h_i/\Delta p$ at a low flow rate of 5 lpm. It is also observed that at the low flow rate, Al_2O_3 and Al_2O_3+ PCM of 0.01% volume concentration nanofluid have lower $h_i/\Delta p$ than DI water irrespective of the increase in heat transfer coefficient, due to the fact that the pressure drop increment dominants over the heat transfer coefficient at a low flow rate. As shown in Figure 11, the total entropy generation rises with an increase in the flow rate of nanofluid. With

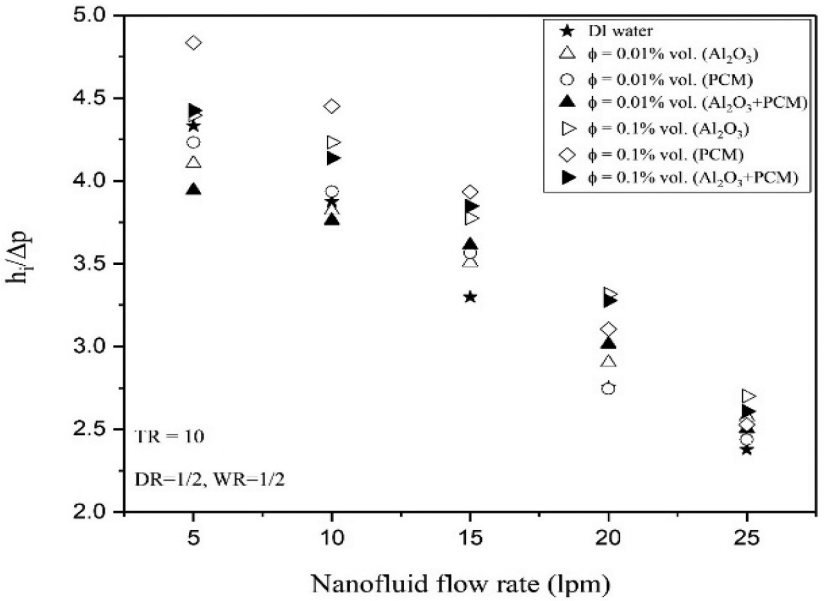

Figure 10. Variation of ratio h/Δp with nanofluid flow rate for different volume concentrations.

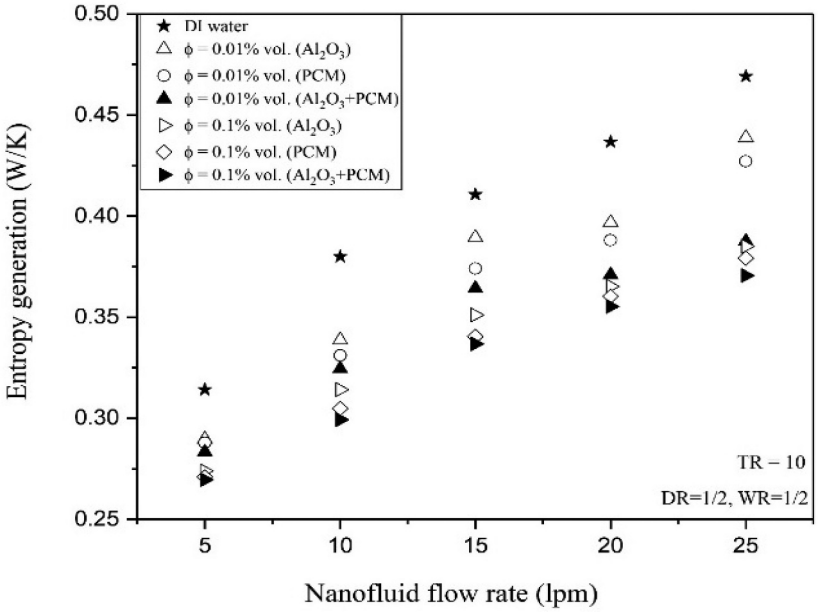

Figure 11. Variation of entropy generation with nanofluid flow rate for different volume concentrations.

Table 4. Comparison of performance enhancements as compared to water in plain tube (h = 3540.6 W/m^2 K, Nu = 106.6, Δp = 1000 Pa, f = 0.02301, h/Δp = 3.53 and S_{gen} = 0.4692) for twisting ratio = 10, depth ratio = 1/2, width ratio = 1/2 and inlet temperature = 30°C.

	Plain tube		Plain twisted tape		V-cut twisted tape	
Parameters	0.01%	0.1%	0.01%	0.1%	0.01%	0.1%
h	22.48%	30.76%	25.53%	35.59%	28.88%	36.24%
Nu	22.12%	30.24%	25.28%	35.04%	28.56%	35.73%
Δp	37.68%	44.05%	51.69%	58.94%	58.62%	59.28%
f	36.51%	45.22%	46.51%	58.54%	54.53%	59.49%
h/Δp	29.97%	46.52%	48.59%	52.85%	68.38%	54.96%
S_{gen}	4.15% (reduction)	6.79% (reduction)	7.30% (reduction)	10.85% (reduction)	14.92% (reduction)	21.94% (reduction)

increase the volume concentration from 0.01% to 0.1%, entropy generation decreases. Addition of solid nanoparticles in the base fluid leads to a decrease in the effective temperature differences and an increase in the pressure drop and thus significantly decreases the total entropy generation. Also, the entropy generation of all working fluids is less than that of the DI water. In comparison to DI water, using V-cut twisted tape of the same twist ratio of 10 and the same depth and width ratios (DR = 1/2, WR = 1/2), total entropy generation reduces by 21.94% and 14.92% for Al_2O_3+ PCM hybrid nanofluid of 0.1% and 0.01% volume concentrations, respectively (Table 4).

Effect of tape twisting ratio

Figures 12 and 13 demonstrate the effect of twisting ratio of the V-cut twisted tape inserts on the heat transfer and pressure drop characteristics for the same volume concentration (ϕ = 0.1%) and depth and width ratios (DR = 1/2, WR = 1/2). Heat transfer coefficient (h_i) and pressure drop (Δp) increase with the increase in nanofluid flow rate for all working fluids. Also, the results reveal that h_i and Δp increase with decreasing the twist ratio. This can be explained by the fact that with decreasing the twist

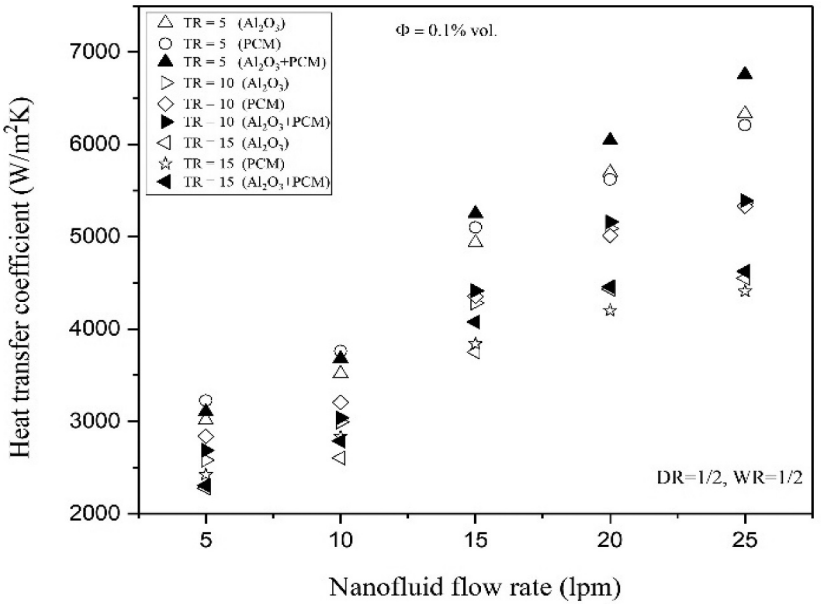

Figure 12. Variation of heat transfer coefficient with nanofluid flow rate for different TR.

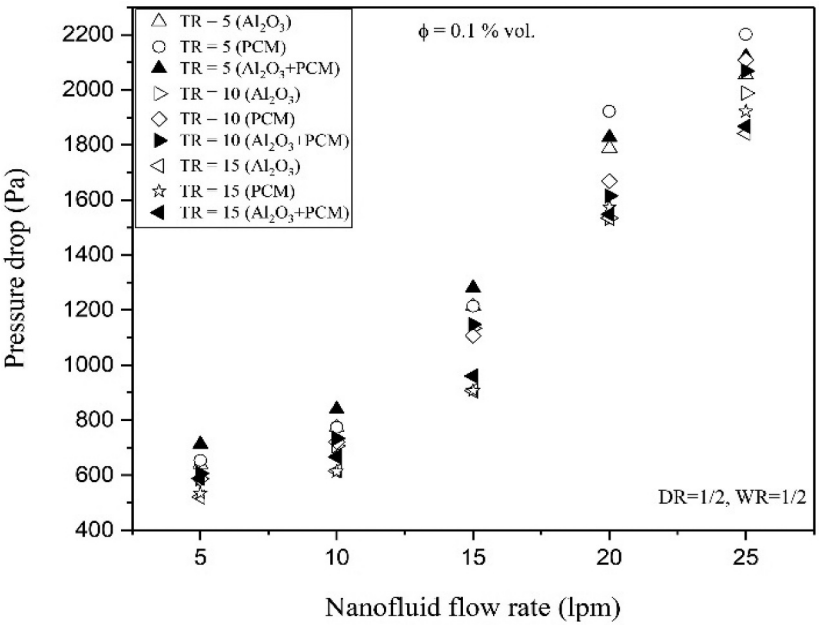

Figure 13. Variation of pressure drop with nanofluid flow rate for different TR.

ratio, it raises the swirl flow, which creates a better mixing of the fluid. This swirl flow diminishes the boundary layer thickness and increases flow turbulence intensity, which leads to greater heat transfer along with the penalty of pressure drop. For the given TR of 5 and flow rate of 25 lpm, the maximum value of h_i is observed as 6757 W/m^2 K for Al_2O_3+ PCM followed by Al_2O_3 (6330.2 W/m^2 K) and PCM (6210 W/m^2 K) hybrid nanofluids and the maximum value of Δp is observed as 2201.3 Pa for PCM, followed by Al_2O_3+ PCM (2121.3 Pa) and Al_2O_3 (2054.6 Pa) hybrid nanofluids, respectively. As

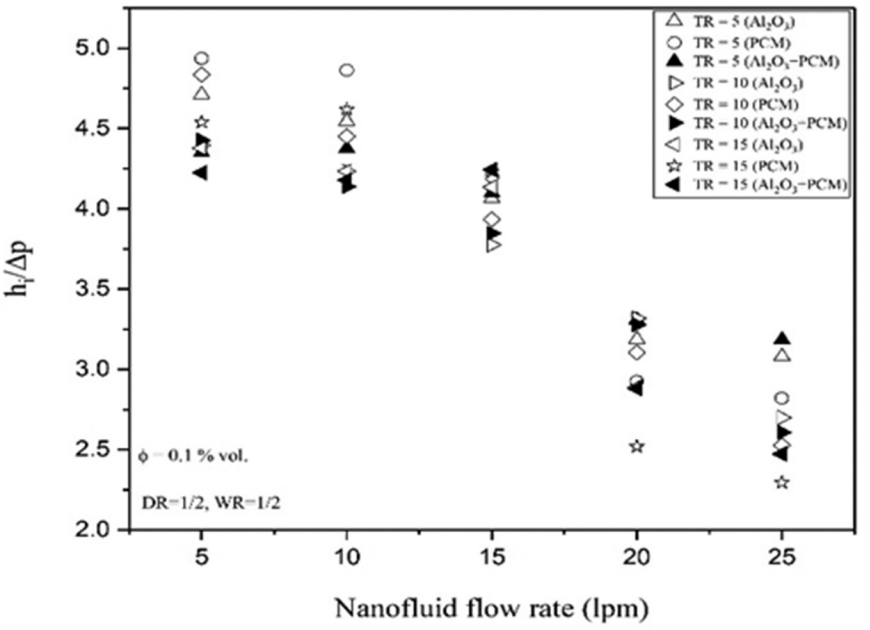

Figure 14. Variation of ratio h/Δp with nanofluid flow rate for different TR.

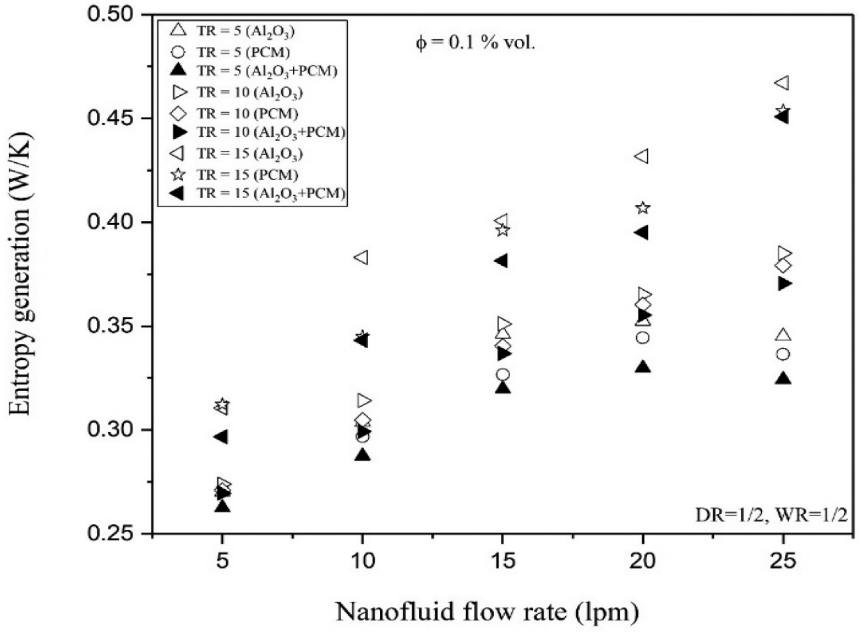

Figure 15. Variation of entropy generation with nanofluid flow rate for different TR.

previously mentioned, PCM shows a higher h_i at a low flow rate and Δp at a higher flow rate. For Al_2O_3+ PCM hybrid nanofluid, the average values of h_i and Δp at TR = 5, 10 and 15 are 47.62%, 36.24% and 27.81% and 63.69%, 59.49% and 55.82%, respectively, greater than those in the tube without tape using DI water.

Figures 14 and 15 predict the variations of $h_i/\Delta p$ ratio and entropy generation with respect to nanofluid flow rate for the same volume concentration ($\phi = 0.1\%$) and depth and width ratio (DR = 1/2, WR = 1/2). The $h_i/\Delta p$ ratio decreases with an increase in the nanofluid flow rate for all cases of working fluids. The $h_i/\Delta p$ ratio shows the maximum value at a low flow rate for PCM using V-cuts twisted tape of TR = 5. It is due to the fact that for the same twist ratio, the increment in h_i dominants over the Δp. At a higher flow rate, increment in pressure drop dominants over the heat transfer coefficient; therefore, Al_2O_3+ PCM shows the minimum value of $h_i/\Delta p$ for TR = 5. In Figure 15, the total entropy generation rises with an increase in twist ratio for all working fluids. Using V-cut twisted tape of TR = 15, Al_2O_3 shows maximum entropy generation while Al_2O_3+ PCM shows minimum entropy generation when V-cut twisted tape of TR = 5 is used. In comparison to TR = 15 using Al_2O_3+ PCM hybrid nanofluid, using V-cut twisted tape of the same depth and width ratios (DR = 1/2, WR = 1/2), the result found 17.69% reduction in total entropy generation for TR = 5 of and 12.30% for TR = 10, respectively.

Effects of depth ratio and width ratio

Figures 16 and 17 show the effects of depth and width ratio of V-cuts twisted tape on the heat transfer coefficient and pressure for the same volume concentration ($\phi = 0.1\%$) and mean twist ratio, TR = 10. The results reveal that both h_i and Δp increase with a decrease in width ratio and increase in depth ratio for all the working fluids. The reason for this enhancement can be explained as for higher DR and lower WR, the vorticity behind the cuts develops extra turbulence and enhances the heat transfer rate with the penalty of Δp. For the same DR of 1/2, WR of 1/3 and flow rate of 25 lpm, the maximum value of heat transfer coefficient is observed 5746.4 W/m^2 K for Al_2O_3+ PCM, followed by PCM (5612.8 W/m^2 K) and Al_2O_3 (5528.5 W/m^2 K) hybrid nanofluid and the maximum value of pressure drop is observed 2134.6 Pa for PCM followed by Al_2O_3+ PCM (2067.9 Pa) and Al_2O_3 (2001.2 Pa) hybrid nanofluids, respectively. For Al_2O_3+ PCM hybrid nanofluid, the average h_i and Δp for V-cuts twisted tape of DR = 1/2 and WR = 1/3 are enhanced around 9.20% and 9.85 %, respectively, when compared to V-cuts twisted tape of DR = 1/3 and WR = 1/2 at the flow rate range of 5–25 lpm. It can be

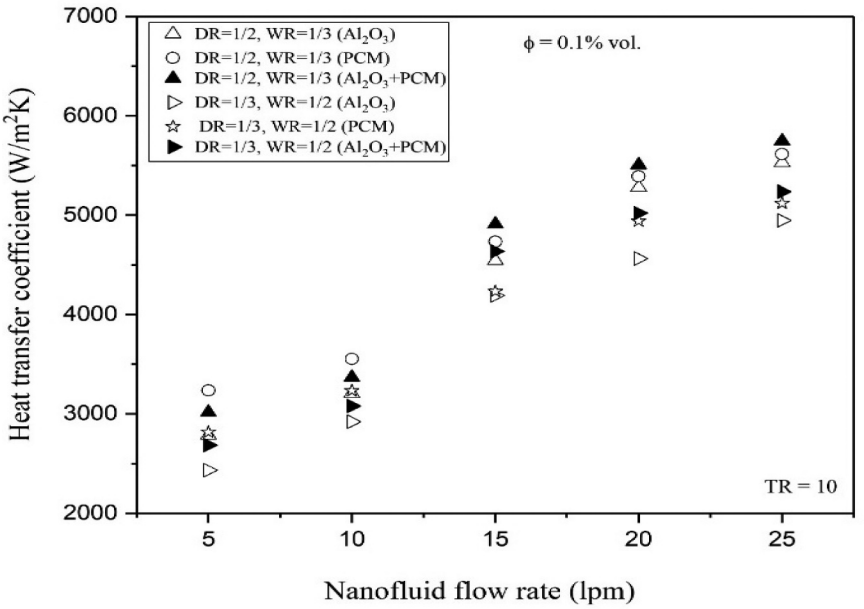

Figure 16. Variation of heat transfer coefficient with flow rate for different DR and WR.

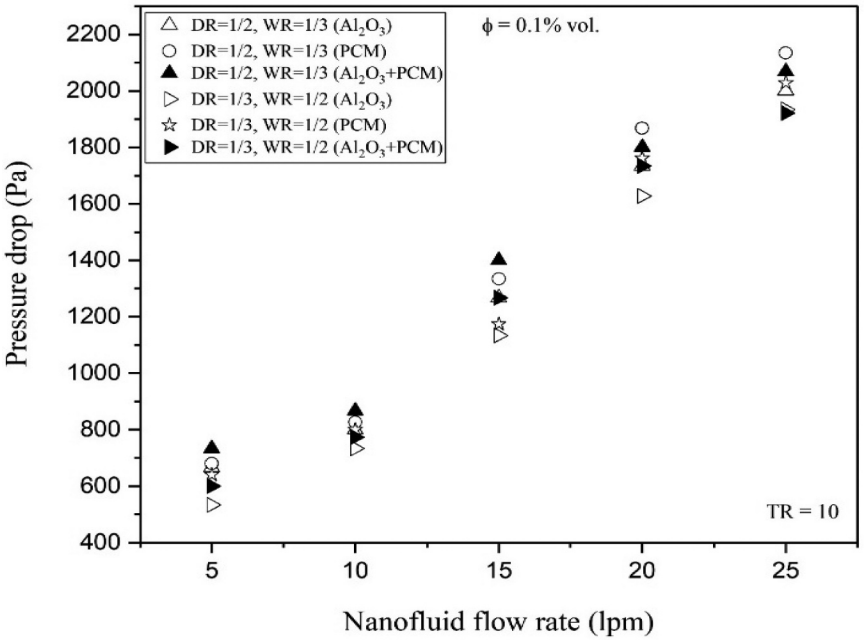

Figure 17. Variation of pressure drop with nanofluid flow rate for different DR and WR.

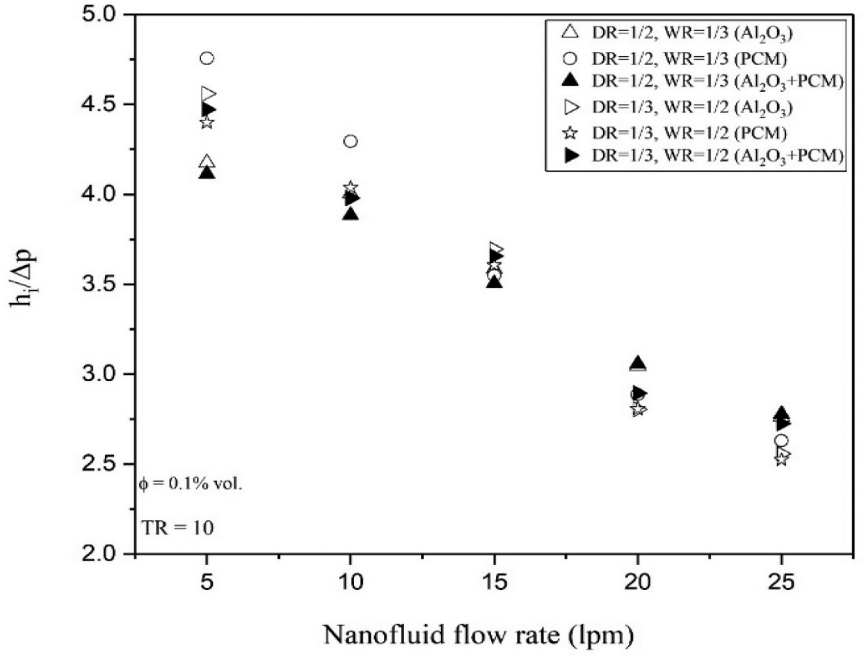

Figure 18. Variation of ratio h/Δp with nanofluid flow rate for different DR and WR.

concluded that the higher depth ratio (i.e., DR = 1/2) and lower width ratio (i.e., WR = 1/3) yield higher heat transfer rate with the penalty of Δp than those of V-cuts twisted tape with lower depth ratio (i.e., DR = 1/3) and higher width ratio (i.e., WR = 1/2).

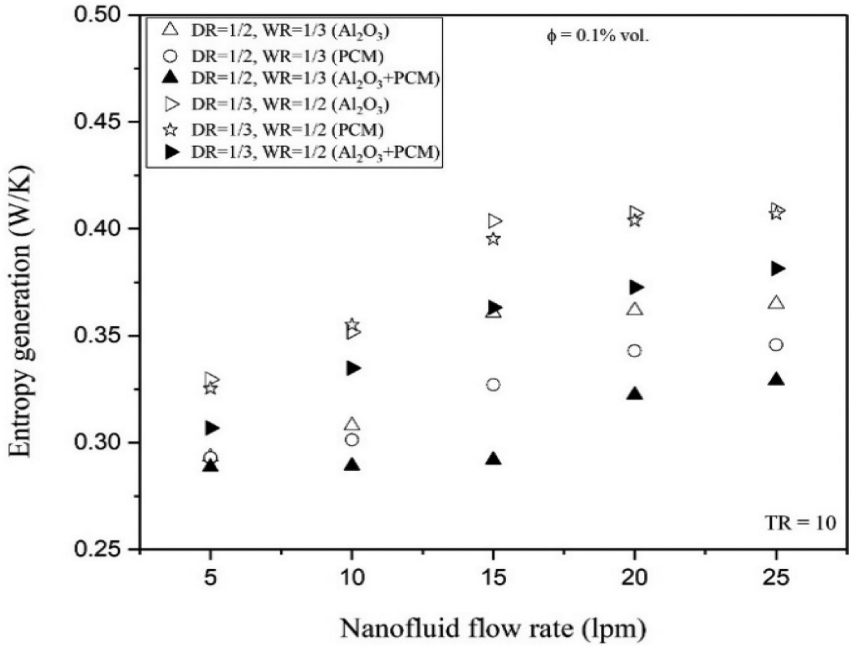

Figure 19. Variation of entropy generation with nanofluid flow rate for different TR.

Figures 18 and 19 predict the variations of the $h_i/\Delta p$ ratio and entropy generation with respect to the nanofluid flow rate for the same volume concentration (ϕ = 0.1%) and mean twist ratio, TR = 10. As expected, the ratio $h_i/\Delta p$ decreases with an increase in the nanofluid flow rate for all cases of working fluids. The ratio $h_i/\Delta p$ shows the maximum value for PCM at a low flow rate and Al_2O_3+ PCM at a high flow rate using V-cuts twisted tape of DR = 1/2, WR = 1/3. At the low flow rate, with the V-cuts twisted tape of DR = 1/3, WR = 1/2, the ratio $h_i/\Delta p$ exhibits higher value than that of V-cuts twisted tape of DR = 1/2, WR = 1/3 as the pressure drop is low at the low flow rate. In Figure 19, the total entropy generation increases with a decrease in DR and an increase in WR for all working fluids. Using V-cut twisted tape of DR = 1/3, WR = 1/2, Al_2O_3shows maximum entropy generation while Al_2O_3+ PCM shows minimum entropy generation when V-cut twisted tape of DR = 1/2, WR = 1/3 is used. In comparison to DR = 1/3 and WR = 1/2 using Al_2O_3+ PCM hybrid nanofluid, using V-cut twisted tape of the same twist ratio TR = 10, the result is observed as 13.29% reduction in total entropy generation for DR = 1/2, WR = 1/3.

Conclusions

Experimental analysis for hydrothermal performance and entropy generation rate of the concentric tube heat exchanger with V-cut twisted tape inserts having twist ratio of 5, 10, and 15 and different depth and width ratio (DR = 1/2 and 1/3, WR = 1/2 and 1/3) using different nanofluids (Al_2O_3, PCM and Al_2O_3+PCM) at volume concentrations of 0.01% and 0.1% was conducted under turbulent flow condition. Following conclusions can be drawn:

- The heat transfer coefficient and pressure drop of nanofluids considerably increases with the flow rate. In addition, both are higher than those of DI water and enhance with volume concentration. Again both increase with the decrease in twist ratio, increase in DR and decrease in WR in the case of all working fluids.

- At a flow rate of 25 lpm and 0.1% volume concentration, heat transfer coefficient increment is maximum (25.6%) for Al_2O_3+ PCM nanofluid and pressure drop increment is maximum (16.05%) for PCM nanofluids as compared to water.
- For Al_2O_3+ PCM hybrid nanofluid, increments of heat transfer coefficient and pressure drop at TR of 5, 10, and 15 are 47.62%, 36.24% and 27.81% and 63.69%, 59.49% and 55.82%, respectively.
- The $h_i/\Delta p$ ratio decreases with an increase in the nanofluid flow rate for all cases of working fluids. Among all working fluids, PCM nanofluid shows maximum $h_i/\Delta p$ at a low flow rate. Within studied ranges, the $h_i/\Delta p$ ratio shows the maximum value at a low flow rate for PCM nanofluid using V-cuts twisted tape of TR = 5.
- The entropy generation of all nanofluids is less than that of DI water. For TR of 10, DR of 1/2 and WR of 1/2, the total entropy generation rate reduces by 21.94% and 14.92% for Al_2O_3+ PCM hybrid nanofluid of 0.1% and 0.01%, respectively.

Nomenclature

c_p: Specific heat capacity ($J.kg^{-1}.K^{-1}$)
d: Tube diameter (m)
D: Width of the twisted tape (m)
f: Friction factor
h: Heat transfer coefficient ($W.K^{-1}.m^{-2}$)
H: Pitch of the twisted tape (m)
k: Thermal conductivity ($W.K^{-1}.m^{-1}$)
Nu: Nusselt number
L: Effective tube length (m)
m: Mass flow rate ($kg.s^{-1}$)
Pr: Prandtl number
Q: Heat transfer rate (W)
Re: Reynolds number
S_{gen}: Entropy generation ($W.K^{-1}$)
T: Temperature (K)
$\dot{V}$: Volume flow rate (lpm)
v: Fluid velocity ($m.s^{-1}$)

Greek Symbols

$\emptyset$: Particle volume concentration
μ: Dynamic viscosity (Pa.s)
ρ: Density ($kg.m^{-3}$)
Δp: Pressure drop (Pa)

Subscripts

avg: average
c: cold fluid
h: hot fluid
hnf: mono/hybrid nanofluid
i, o: inner, outer
in, out: inlet, outlet
it, ot: inner tube, outer tube
w: tube wall

Abbreviations

DR: Depth ratio
LMTD: Log mean temperature difference
TR: Twist ratio
WR: Width ratio

References

[1] S. Eiamsa-Ard, V. Kongkaitpaiboon, and P. Promvonge, "Thermal performance assessment of turbulent tube flow through wire coil turbulators," *Heat Transfer Eng.*, vol. 32, no. 11–12, pp.957–967, 2011. DOI: 10.1080/01457632.2011.556381.

[2] M. C. S. Reddy and V. V. Rao, "Experimental investigation of heat transfer coefficient and friction factor of ethylene glycol water based TiO_2 nanofluid in double pipe heat exchanger with and without helical coil inserts," *Int. Commun. Heat Mass Transf.*, vol. 50, pp. 68–76, 2014. DOI: 10.1016/j.icheatmasstransfer.2013.11.002.

[3] M. T. Naik, S. S. Fahad, L. S. Sundar, and M. K. Singh, "Comparative study on thermal performance of twisted tape and wire coil inserts in turbulent flow using CuO/water nanofluid," *Exp. Therm. Fluid Sci.*, vol. 57, pp. 65–76, 2014. DOI: 10.1016/j.expthermflusci.2014.04.006.

[4] H. A. Mohammed, H. A. Hasan, and M. A. Wahid, "Heat transfer enhancement of nanofluids in a double pipe heat exchanger with louvered strip inserts," *Int. Commun. Heat Mass Transf.*, vol. 40, pp. 36–46, 2013. DOI: 10.1016/j.icheatmasstransfer.2012.10.023.

[5] N. T. R. Kumar, P. Bhramara, L. S. Sundar, M. K. Singh, and A. C. M. Sousa, "Heat transfer, friction factor and effectiveness of Fe_3O_4 nanofluid flow in an inner tube of double pipe U-bend heat exchanger with and without longitudinal strip inserts," *Exp. Therm. Fluid Sci.*, vol. 85, pp. 331–343, 2017. DOI: 10.1016/j.expthermflusci.2017.03.019.

[6] M. Arulprakasajothi, K. Elangovan, U. Chandrasekhar, and S. Suresh, "Performance study of conical strip inserts in tube heat exchanger using water based titanium oxide nanofluid," *Therm Sci.*, vol. 22, pp. 477–485, 2018. DOI: 10.2298/TSCI151024250A.

[7] C. Muthusamy, M. Vivar, I. Skryabin, and K. Srithar, "Effect of conical cut-out turbulators with internal fins in a circular tube on heat transfer and friction factor," *Int. Commun. Heat Mass Transf.*, vol. 44, pp. 64–68, 2013. DOI: 10.1016/j.icheatmasstransfer.2013.03.004.

[8] H. A. Mohammed, I. A. M. A. Abuobeida, H. B. Vuthaluru, and S. Liu, "Two-phase forced convection of nanofluids flow in circular tubes using convergent and divergent conical rings inserts," *Int. Commun. Heat Mass Transf.*, vol. 101, pp. 10–20, 2019. DOI: 10.1016/j.icheatmasstransfer.2018.12.010.

[9] A. T. Wijayanta, T. Istanto, K. Kariya, and A. Miyara, "Heat transfer enhancement of internal flow by inserting punched delta winglet vortex generators with various attack angles," *Exp. Therm. Fluid Sci.*, vol. 87, pp. 141–148, 2017. DOI: 10.1016/j.expthermflusci.2017.05.002.

[10] Y. Lei, F. Zheng, C. Song, and Y. Lyu, "Improving the thermal hydraulic performance of a circular tube by using punched delta-winglet vortex generators," *Int. J. Heat Mass Transfer*, vol. 111, pp. 299–311, 2017. DOI: 10.1016/j.ijheatmasstransfer.2017.03.101.

[11] A. T. Wijayanta, I. Yaningsih, M. Aziz, T. Miyazaki, and S. Koyama, "Double-sided delta-wing tape inserts to enhance convective heat transfer and fluid flow characteristics of a double-pipe heat exchanger," *Appl. Therm. Eng.*, vol. 145, pp. 27–37, 2018. DOI: 10.1016/j.applthermaleng.2018.09.009.

[12] D. Kumar, A. K. Patil, and M. Kumar, Experimental investigation of heat transfer and fluid flow in a circular tube with lanced ring insert, *Exp. Heat Transfer.*, pp. 1–12, in press 2019. DOI:10.1080/08916152.2019.1691086.

[13] S. Pourahmad, S. M. Pesteei, and M. Mehrabi, "The effect of geometrical characteristics of wavy strip turbulator and thermodynamic properties of fluid on exergy loss and heat transfer in a tube in tube heat exchanger," *Exp. Heat Transfer.*, vol. 32, no. 4, pp.393–409, 2019. DOI: 10.1080/08916152.2018.1526229.

[14] A. R. S. Suri, A. Kumar, and R. Maithani, "Experimental determination of enhancement of heat transfer in a multiple square perforated twisted tape inserts heat exchanger tube," *Exp. Heat Transfer*, vol. 31, no. 2, pp.85–105, 2018. DOI: 10.1080/08916152.2017.1397814.

[15] S. Ponnada, T. Subrahmanyam, and S. V. Naidu, "A comparative study on the thermal performance of water in a circular tube with twisted tapes, perforated twisted tapes and perforated twisted tapes with alternate axis," *Int. J. Therm. Sci.*, vol. 136, pp. 530–538, 2019. DOI: 10.1016/j.ijthermalsci.2018.11.008.

[16] S. M. Abolarin, M. Everts, and J. P. Meyer, "Heat transfer and pressure drop characteristics of alternating clockwise and counter clockwise twisted tape inserts in the transitional flow regime," *Int. J. Heat Mass Transfer*, vol. 133, pp. 203–217, 2019. DOI: 10.1016/j.ijheatmasstransfer.2018.12.107.

[17] R. Datt, M. S. Bhist, A. D. Kotiyal, R. Maithani, and A. Kumar, "Development of new correlations for heat transfer and friction loss of solid ring with combined square wing twisted tape inserts heat exchanger tube," *Exp. Heat Transfer*, vol. 32, no. 2, pp.179–200, 2019. DOI: 10.1080/08916152.2018.1505784.

[18] K. Ruengpayungsak, M. Kumar, V. Chuwattanakul, and S. Eiamsa-ard, "Experimental study of the effects of inclusion of rectangular-cut twisted tapes on heat transfer and pressure drop in a round tube," *Arabian J. Sci. Eng.*, vol. 44, no. 12, pp.10303–10312, 2019. DOI: 10.1007/s13369-019-04047-7.

[19] H. G. Langeroudi and K. Javaherdeh, "Investigation friction factor and heat transfer characteristics of turbulent flow inside the corrugated tube inserted with typical and V-cut twisted tapes," *Heat Mass Transfer.*, vol. 54, no. 7, pp.1999–2008, 2018. DOI: 10.1007/s00231-018-2288-4.

[20] B. Kumar, M. Kumar, A. K. Patil, and S. Jain, "Effect of V cut in perforated twisted tape insert on heat transfer and fluid flow behavior of tube flow: An experimental study," *Exp. Heat Transfer.*, vol. 32, no. 6, pp.524–544, 2019. DOI: 10.1080/08916152.2018.1545808.

[21] H. G. Langeroudi and K. Javaherdeh, "Experimental study of non-Newtonian fluid flow inside the corrugated tube inserted with typical and V-cut twisted tapes," *Heat and Mass Transfer.*, vol. 55, no. 4, pp.937–951, 2019. DOI: 10.1007/s00231-018-2467-3.

[22] B. Kumar, A. K. Patil, S. Jain, and M. Kumar, "Study of entropy generation in heat exchanger tube with multiple V cuts in perforated twisted tape insert," *J. Heat Transfer*, vol. 141, no. 8, pp.081801, 2019. DOI: 10.1115/1.4043769.

[23] W.-X. Chu, C. Tsai, B.-H. Lee, K.-Y. Cheng, and C.-C. Wang, "Experimental investigation on heat transfer enhancement with twisted tape having various V-cut configurations," *Appl. Therm. Eng.*, vol. 172, pp. 115148, 2020. DOI: 10.1016/j.applthermaleng.2020.115148.

[24] B. Kumar, A. K. Patil, S. Jain, and M. Kumar, Effects of double V cuts in perforated twisted tape insert: An experimental study, *Heat Transf. Eng.*, in press 2019.

[25] A. Kumar, S. Singh, S. Chamoli, and M. Kumar, "Experimental investigation on thermo-hydraulic performance of heat exchanger tube with solid and perforated circular disk along with twisted tape insert," *Heat Transfer Eng.*, vol. 40, no. 8, pp.616–626, 2019. DOI: 10.1080/01457632.2018.1436618.

[26] A. Wahab, *et al.*, "Solar energy systems – potential of nanofluids," *J. Mol. Liq.*, vol. 289, pp. 111049, 2019. DOI: 10.1016/j.molliq.2019.111049.

[27] N. Abbas, *et al.*, "Applications of nanofluids in photovoltaic thermal systems: A review of recent advances," *Physica A*, vol. 536, pp. 122513, 2019. DOI: 10.1016/j.physa.2019.122513.

[28] T. R. Shah and H. M. Ali, "Applications of hybrid nanofluids in solar energy, practical limitations and challenges: A critical review," *Sol. Energy*, vol. 183, pp. 173–203, 2019. DOI: 10.1016/j.solener.2019.03.012.

[29] M. Ahmadlouydarab, M. Ebadolahzadeh, and H. M. Ali, "Effects of utilizing nanofluid as working fluid in a lab-scale designed FPSC to improve thermal absorption and efficiency," *Physica A*, vol. 540, pp. 123109, 2020. DOI: 10.1016/j.physa.2019.123109.

[30] A. Khan, *et al.*, "Experimental investigation of enhanced heat transfer of a car radiator using ZnO nanoparticles in H_2O–ethylene glycol mixture," *J. Therm. Anal. Calorim.*, vol. 138, no. 5, pp.3007–3021, 2019. DOI: 10.1007/s10973-019-08320-7.

[31] S. Javed, *et al.*, "Internal convective heat transfer of nanofluids in different flow regimes: A comprehensive review," *Physica A*, vol. 538, no. 122783, pp.122783, 2020. DOI: 10.1016/j.physa.2019.122783.

[32] T. Ambreen, A. Saleem, H. M. Ali, S. A. Shehzad, and C. W. Park, "Performance analysis of hybrid nanofluid in a heat sink equipped with sharp and streamlined micro pin-fins," *Powder Technology*, vol. 355, pp. 552–563, 2019. DOI: 10.1016/j.powtec.2019.07.087.

[33] A. K. Hussein, *et al.*, "Mixed convection in a cubical cavity with active lateral walls and filled with hybrid graphene–platinum nanofluid," *J. Therm. Sci. Eng. Appl.*, vol. 11, no. 4, pp.1–9, 2019. DOI: 10.1115/1.4043758.

[34] M. Sahu and J. Sarkar, "Steady-state energetic and exergetic performances of single-phase natural circulation loop with hybrid nanofluids," *J. Heat Transfer*, vol. 141, no. 8, pp.082401, 2019. DOI: 10.1115/1.4043819.

[35] S. K. Singh and J. Sarkar, "Improvement in energy performance of tubular heat exchangers using nanofluids: A review," *Curr. Nanosci.*, vol. 16, no. 2, pp.136–156, 2020. DOI: 10.2174/1573413715666190715101044.

[36] S. Doruk, O. N. Şara, A. Karaipekli, and S. Yapıcı, "Heat transfer performance of water and nanoencapsulated n-nonadecane based nanofluids in a double pipe heat exchanger," *Heat Mass Transf.*, vol. 53, no. 12, pp.3399–3408, 2017. DOI: 10.1007/s00231-017-2072-x.

[37] V. Mikkola, S. Puupponen, K. Saari, T. Ala-Nissila, and A. Seppala, "Thermal properties and convective heat transfer of phase changing paraffin nanofluids," *Int. J. Therm. Sci.*, vol. 117, pp. 163–171, 2017. DOI: 10.1016/j.ijthermalsci.2017.03.024.

[38] H. Maddah, M. Alizadeh, N. Ghasemi, and S. R. W. Alwi, "Experimental study of Al_2O_3/water nanofluid turbulent heat transfer enhancement in the horizontal double pipes fitted with modified twisted tapes," *Int. J. Heat Mass Transfer*, vol. 78, pp. 1042–1054, 2014. DOI: 10.1016/j.ijheatmasstransfer.2014.07.059.

[39] E. Esmaeilzadeh, H. Almohammadi, A. Nokhosteen, A. Motezaker, and A. N. Omrani, "Study on heat transfer and friction factor characteristics of γ-Al_2O_3/water through circular tube with twisted tape inserts with different thicknesses," *Int. J. Therm. Sci.*, vol. 82, pp. 72–83, 2014. DOI: 10.1016/j.ijthermalsci.2014.03.005.

[40] P. V. D. Prasad, A. V. S. S. K. S. Gupta, and K. Deepak, "Investigation of trapezoidal-cut twisted tape insert in a double pipe U-tube heat exchanger using Al_2O_3/water nanofluid," *Procedia Mater. Sci.*, vol. 10, pp. 50–63, 2015. DOI: 10.1016/j.mspro.2015.06.025.

[41] M. Hazbehian, H. Maddah, H. Mohammadiun, and M. Alizadeh, "Experimental investigation of heat transfer augmentation inside double pipe heat exchanger equipped with reduced width twisted tapes inserts using polymeric nanofluid," *Heat and Mass Transfer*, vol. 52, no. 11, pp.2515–2529, 2016. DOI: 10.1007/s00231-016-1764-y.

[42] M. E. Nakhchi and J. A. Esfahani, "Cu-water nanofluid flow and heat transfer in a heat exchanger tube equipped with cross-cut twisted tape," *Powder Technol.*, vol. 339, pp. 985–994, 2018. DOI: 10.1016/j.powtec.2018.08.087.

[43] M. Khoshvaght-Aliabadi, S. Davoudi, and M. H. Dibaei, "Performance of agitated-vessel U tube heat exchanger using spiky twisted tapes and water based metallic nanofluids," *Chem. Eng. Res. Design*, vol. 133, pp. 26–39, 2018. DOI: 10.1016/j.cherd.2018.02.030.

[44] M. Bahiraei, N. Mazaheri, and F. Aliee, "Second law analysis of a hybrid nanofluid in tubes equipped with double twisted tape inserts," *Powder Technol.*, vol. 345, pp. 692–703, 2019. DOI: 10.1016/j.powtec.2019.01.060.

[45] S. Eiamsa-ard, K. Wongcharee, K. Kunnarak, M. Kumar, and V. Chuwattabakul, "Heat transfer enhancement of TiO2-water nanofluid flow in dimpled tube with twisted tape insert," *Heat Mass Transfer*, vol. 55, no. 10, pp.2987–3001, 2019. DOI: 10.1007/s00231-019-02621-1.
[46] S. K. Singh and J. Sarkar, Improving hydrothermal performance of double-tube heat exchanger with modified twisted tape inserts using hybrid nanofluid, *J. Therm. Anal. Calorim.*, in press 2020. DOI:10.1007/s10973-020-09380-w.
[47] J. Dirker and J. P. Meyer, "Heat transfer coefficients in concentric annuli," *J. Heat Transfer*, vol. 124, no. 6, pp.1200–1202, 2002. DOI: 10.1115/1.1517266.
[48] S. J. Kline and F. A. McClintock, "Describing uncertainties in single-sample experiments," *Mech. Eng.*, vol. 75, pp. 3–8, 1953.
[49] F. P. Incropera, P. D. DeWitt, T. L. Bergman, and A. S. Lavine. *Fundamentals of Heat and Mass Transfer*. John-Wiley & Sons, USA, 2006.
[50] K. Nanan, C. Thianpong, P. Promvonge, and S. Eiamsa-ard, "Investigation of heat transfer enhancement by perforated helical twisted-tapes," *Int. Commun. Heat Mass Transf.*, vol. 52, pp. 106–112, 2014. DOI: 10.1016/j.icheatmasstransfer.2014.01.018.
[51] R. M. Manglik and A. E. Bergles, "Heat transfer and pressure drop correlations for twisted-tape inserts in isothermal tubes: Part II—Transition and turbulent flows," *J. Heat Transfer*, vol. 115, no. 4, pp.890–896, 1993. DOI: 10.1115/1.2911384.

Appendix A. Uncertainty analysis

- Reynolds number, *Re*;

$$\frac{\Delta \mathrm{Re}}{\mathrm{Re}} = \sqrt{\left(\frac{\Delta \dot{V}}{\dot{V}}\right)^2 + \left(\frac{\Delta \mu}{\mu}\right)^2 + \left(\frac{\Delta \rho}{\rho}\right)^2} \tag{A.1}$$

- Heat transfer rate, *Q*;

$$\frac{\Delta \mathrm{Q}}{Q} = \sqrt{\left(\frac{\Delta \dot{V}}{\dot{V}}\right)^2 + \left(\frac{\Delta \rho}{\rho}\right)^2 + \left(\frac{\Delta \mathrm{cp_h}}{cp_h}\right)^2 + \left(\frac{(\Delta(\mathrm{T_{in}} - \mathrm{T_{out}}))}{(T_{in} - T_{out})}\right)^2} \tag{A.2}$$

- Overall heat transfer coefficient, *U*;

$$\frac{\Delta \mathrm{U}}{U} = \sqrt{\left(\frac{\Delta \mathrm{Q}}{Q}\right)^2 + \left[\frac{\Delta\left(\frac{\left(\mathrm{T_{h,in}} - \mathrm{T_{c,out}}\right) - \left(\mathrm{T_{h,out}} - \mathrm{T_{c,in}}\right)}{\ln\left(\frac{\mathrm{T_{h,in}} - \mathrm{T_{c,out}}}{\mathrm{T_{h,out}} - \mathrm{T_{c,in}}}\right)}\right)}{\left(\frac{\left(T_{h,in} - T_{c,out}\right) - \left(T_{h,out} - T_{c,in}\right)}{\ln\left(\frac{T_{h,in} - T_{c,out}}{T_{h,out} - T_{c,in}}\right)}\right)}\right]^2} \tag{A.3}$$

- Nusselt number, *Nu*;

$$\frac{\Delta \mathrm{Nu}}{Nu} = \sqrt{\left(\frac{\Delta \mathrm{h}}{h}\right)^2 + \left(\frac{\Delta \mathrm{k}}{k}\right)^2} \tag{A.4}$$

- Friction factor, *f*;

$$\frac{\Delta \mathrm{f}}{f}=\sqrt{\left(\frac{\Delta(\Delta \mathrm{p})}{\Delta \mathrm{p}}\right)^{2}+\left(\frac{\Delta \rho}{\rho}\right)^{2}+\left(\frac{2 \Delta \mathrm{v}}{\nu}\right)^{2}} \tag{A.5}$$

- Entropy generation ratio S_{gen};

$$\frac{\Delta \mathrm{S}_{\mathrm{gen}}}{S_{gen}}=\sqrt{\left(\frac{\Delta \dot{V}}{\dot{V}}\right)^{2}+\left(\frac{\Delta \mathrm{cp}}{cp}\right)^{2}+\left(\frac{\Delta \ln\left(\frac{\mathrm{T}_{\mathrm{out}}}{\mathrm{T}_{\mathrm{in}}}\right)}{\ln\left(\frac{T_{out}}{T_{in}}\right)}\right)^{2}+\left(\frac{\Delta \Delta \mathrm{P}}{\Delta \mathrm{P}}\right)^{2}+2\left(\frac{\Delta \rho}{\rho}\right)^{2}+\left(\frac{\Delta \mathrm{T}_{\mathrm{avg}}}{T_{avg}}\right)^{2}} \tag{A.6}$$